Proceedings of the ASME 2021
Manufacturing Science and Engineering Conference
MSEC2021
Jun 21-25, 2021, Cincinnati, Ohio, USA

MSEC2021-60520

A NOVEL PACKING HOLLOW DODECAHEDRON MODEL TO STUDY THE MECHANICAL AND THERMAL PROPERTIES OF STOCASTIC METALLIC FOAMS

Rui Dai, Beomjin Kwon, Qiong Nian[1]

[1]Department of Aerospace and Mechanical Engineering
Arizona State University
Tempe, AZ

ABSTRACT

Cellular metamaterials have been extensively studied and offer distinguished physical properties to be used in various fields, e.g., heat exchanger, battery electrodes, automotive, magnetic shielding, catalyst and etc. Stochastic foam architecture as one of the subsets, shows competitive potential due to the easy manufacturing, high strength to weight ratio, super lightweight and super large specific area. The more advanced hollow cellular (shellular) architectures with well-developed structure connections are proposed and expected to surpass the solid micro/nanolattices. However, in terms of theoretical predicting and studying of the cellular foam architecture, currently no systematic model to be utilized to accurately capture both its mechanical and thermal properties especially with hollow strut due to complexity induced by its stochastic and highly reticulate nature. Herein, for the first time, a novel packing three-dimensional (3D) hollow dodecahedron (HPD) model is proposed to simulate the cellular architecture. In addition, an electrochemical deposition process is utilized to manufacture the metallic foam with hollow strut. Mechanical and thermal testing of the as-manufactured foams are carried out. The mechanical strength and the thermal conductivity relationship are studied as the example to verify the proposed 3D packing HPD model.

Keywords: Metamaterial, Cellular structure, Metallic foam, Hollow strut; Pentagonal dodecahedron; Thermal Conductivity; Mechanical Property

NOMENCLATURE

A	area [m^2]
ρ'	relative density
ρ	density of foam [kg/m^3]
ρ_s	density of base material [kg/m^3]
k	thermal conductivity [W/(m·K)]
l	strut length [m]
l_w	strut width [m]
L_i	height of each layer [m]
Q	Joule heating [J]
R	radius of the inscribed sphere [m]
T	temperature [k]
V	volume [m^3]
V_i	volume of each layer envelope [m^3]

GREEK LETTERS

β	inclined angle [°]
φ	fraction of the solid phase

SUBSCRIPTS

$cond$	conduction
cs	cross-section
eff	effective
HPD	hollow pentagonal dodecahedron
Ni	nickel
PU	polyurethane
r	radius
s	solid phase
t	total

1. INTRODUCTION

Light-weight metamaterial based on metal, polymer or ceramic materials have been extensively studied, while most of the studies have devoted on studying the physical properties of

Contact Author: qiong.nian@asu.edu

ultralight cellular metallic foam architecture [1]. These cellular metallic materials can be either manufactured through traditional methods, e.g., powder metallurgy [2], injection molding [3], polymer templated deposition[4], or the newly developed additive manufacturing [5] with topology optimization, machine learning or deep learning like composite structure design [6] and gradient mass distribution, and can either be closed or open cell, stochastic, or periodic in architecture [7]. The advances in manufacturing techniques greatly board the applications for using these materials in battery electrode, catalyst devices, heat exchangers and energy absorption [8]. It is noteworthy that in recent years the versatility of manufacturing for various metal alloys (Ni-P, Ni-Cu, Ni-W-P) [11] with electro-chemical co-deposition on polymer templates [12] engenders unbound potential design space by which new cellular metallic material can be created. Those foam architectures made of novel materials (composite) normally processes tailed material properties over the base template materials, e.g., low weight, super large specific surface area, high gas permeability, high strength, noise and energy absorption and etc. [7, 8].

Specifically, for the thermal transport properties, foams offer extremely large surface area, which offers them repelling potential to be candidate for heat exchange and energy storage. However, if the porous medium merely consists of pure polymer foams, the structure generally possesses small k and poor mechanical strength, which are hard to be improved simply by altering the porous structure. To effectively modulate the thermal and mechanical properties of the foams, not only the architecture but also the constituent material needs to be engineered. For polymer foams, conformal metal coating on their ligament surface can be considered as a facile method of enhancing k and mechanical strength without large cost. Metal coating on the polymer foams is usually implemented by a simple electrochemical co-deposition, which is scalable from nano- to macro-scale sizes. And combining strong, corrosion resistive materials can greatly improve the application value. For example, the higher thermal conductivity and light weight nature of the nickel coated polyurethane (PU) (Ni-PU) foam can possibly promote a uniform temperature distribution throughout the structure, thereby conceptually improve the overall efficiency for the catalyst devices [9].

In terms of the mechanical property, it is demonstrated that by incorporating the complex geometry topology, it can easily reach the ultralight density region, while the stiffness stays almost the same. According to the Gibson and Ashby's law, while the space topology is settled, the stiffness of the structure is limited to a certain region, that is the scaling law of the mechanical strength or the elastic modulus vs. the relative density is determined [10, 11]. Therefore, by realizing a metal coated polymer composite architecture, it's capable to achieve better mechanical property than pure polymer structure while keep a much lower relative density than pure metallic one, which preserves the advantages of both materials and breaks the entanglement of weight and thermal conductivity. Besides, Torrents et al. [12] demonstrated that hollow-strut cellular lattices prepared using electroless nickel (Ni) plating on the polymer-based template and following etching process lead to the world's lightest metallic architecture. Although the metallic cellular structure is hollow one, the stiffness and the strength keeps the same and linear slope for stress vs. strain stays as two. Compared with the solid counterpart, at the same relative density level, hollow architecture yields a better mechanical strength and elastic property.

In addition to the exceptional mechanical and thermal properties, considering the good electric conductivity and highly porous essential, for example, the Ni-PU foam can also be used as the electrodes for supercapacitors [13], oil absorption [14], electromagnetic interference shielding [15] and etc. Moreover, considering Ni can be used for CVD coating of graphene, novel reticular graphene foam or aerogel structure can also be created using it as a template, which will dramatically broaden the applications and arouse interests for both material science community and mechanical community.

Over the past decades, extensive efforts have been put into the modeling of physical properties, i.e., elastic stiffness, elastic strength, flow and heat transfer in porous media. As stated earlier, determining the geometric characteristics of metal foam (i.e., specific area, tortuosity, mean pore diameter, etc.) is challenging. The researchers therefore have developed correlations based on a simplified model of the foam geometry with these geometry parameters expressed as a function of e.g., the porosity of the foam. Different models have been considered: cubic unit cell with slender cylinder, honeycomb structure, Kelvin model [16], consisting of six flat quadrilateral and eight hexagonal faces, Weaire-Phelan [17] or a tetrakaidecahedron [18], interconnected hexagonal cells. Using such basic representations of the unit cell, a large number of studies have been carried out to predict the effective thermal conductivity, heat transfer rate, wetting angel or mechanical properties of metallic foam.

Despite a number of studies have been conducted, there are still big challenges related to the structural interpretation of those cellular metallic materials, especially with hollow struts. Specifically, although numerous FEM models have carried to study the ETC of the foam architecture, the options are only Kelvin model [16], Weaire-Phelan model [17], Tetrakaidecahedral model [18] or the X-ray tomography scanned model[19]. However, all of these models are too complex to create a hollow structure for further study of the foam architecture. For example, the X-ray scanned model, which can provide a more detailed topology of the foam geometry, it still inevitably overestimates the mechanical and thermal properties of the foam structure [20-22]. Additionally, no thickness information can be obtained due to the complicated essential of the X-ray scanned geometry and the thickness cannot be tuned once the model is created, therefore, it's nearly impossible to rebuild the hollow architectures with various thickness based on the X-ray scanning. As a result, almost all of the researches only use solid architecture for the X-ray scanned result to study. Our novel 3D packing hollow pentagon model provides a reliable and easy way to study the metal foam architecture. In this work, PD lattice is utilized as a representative unit cell due to the relatively

low specific surface energy, which corresponds to the fact that the evolution of the foam structure always tends to maintain the minimum surface energy and this structure is commonly observed in the actual stochastic metallic foam. Additionally, this specific topology greatly simplifies the derivation process for the relationships of the structure parameters when compared to randomly distributed units. With a novel 3D packing technique, we demonstrated the HPD model is capable to estimate both the mechanical property and effective thermal conductivity (ETC) of the foam architecture with high accuracy and simpler than traditional models. And in the following parts, estimating the mechanical and thermal property for the cellular metallic foam are provided as the two examples.

2. Experimental and Modeling

2.1 Materials and Sample Preparation

Reticulated PU foam (US Plastic Corp, 20 PPI) is utilized as the template. Upon the PU template, electro-chemical co-deposition technique was applied to prepare the hollow Ni and the Ni-PU composite foam structure. The Ni-PU foam is prepared by the following four steps: 1) the PU templates were totally cleaned alternatively with polyacetylene, acetone and deionized water in the ultrasonic bath for more than 10 minutes; 2) to improve and ensure the copper electro-plating quality, the cleaned PU templates were then immersed in the dopamine·HCl solution (~ 3.0 g/L) resulting a thin layer dopamine shell coated homogeneous outside the PU template followed by cleaning with deionized water in the ultrasonic bath and drying in a vacuum at room temperature for over 2hrs; 3) The dopamine treated templates were immersed in a copper (Cu) electroless plating bath (Caswell Inc., NY) for over 30 minutes to create a conductive copper layer (~ 1μm) on the template surface; 4) Finally, Ni electro-deposition is conducted on the conductive Cu coated PU foam to obtain the Ni-PU composite structure with various thickness (relative density) by varying the coating time. For our nickel electro plating, we applied pulse-reverse method with delicate chosen parameters to ensure the best surface quality of the Ni foam. Finally, thermal annealing in inert atmosphere (Ar) is applied to remove the PU core and obtain the hollow architecture (as shown in Fig. 1a).

2.2 Electro-chemical deposition

Electrochemical co-deposition has been developed that eliminates unexpected influences on composite properties during the preparing process. First, electrochemical deposition is a low-temperature and scalable process (at about room temperature) so no diffusion or chemical reaction is allowed between the graphene nanoplates and the metallic matrix, and therefore the inherent properties of both the graphene and the matrix can be preserved. Second, during the electroplating co-deposition process, metallic ions and graphene are driven towards the cathode and deposit onto the cathode simultaneously. Lastly, we apply electro chemical pulse and reverse deposition (PRED) method to prepare the sample surface for characterizations e.g., Raman spectrum, XRD and nanoindentation.

The Ni plating solution consisted of $NiSO_4 \cdot 6H_2O$ ($300\ g/L$), $NiCl_2 \cdot 6H_2O$ ($35 g/L$), H_3BO_3 ($40 g/L$) and a surfactant (sodium dodecylsulphate, SDS, $0.5 g/L$) was stirred continuously for at least 30 min before deposition and during the plating at a rate of 250 rpm. The electroplating solution contents are shown below in Table 1.

Chemical	Condition	Function
Nickel Sulfate	310 g/L	Nickel Source
Nickel Chloride	25 g/L	Nickel Source
H_2SO_4	appropriate	Complexing agent
Boracic acid	35 g/L	Complexing agent
Saccharine	0.1 g/L	Bonding agent
Perform Temperature	45 ^{0}C	Environment
Stirring	250 m	Dispersion

Table 1: Nickel electrolyte solution

2.3 Modeling and FEM Simulation

PD lattice unit cell is chosen as the representative unit cell to replicate the cellular foam architecture. According to previous studies, the relationship between the width l_w of the triangle cross section and the radius of the sphere cavity R satisfies the relationships:

$$n = 0.0254/(1.1135a) \quad (1)$$

$$R = \sqrt{0.25l_w^2 + (1.209a - 0.309l_w)^2} \quad (2)$$

, where n is the pore size per inch (or PPI) and is utilized to determine the unit cell edge length a.

HPD lattice model is built using the commercial software of Creo/CAE 2017. The hollow struts in the corresponding PD lattice is prepared by the following two steps: 1) a solid PD lattice with edge length of 1140.54 μm is created, which is derived based on the 20 PPI PU foam template; 2) a sphere cavity from the center of the PD structure is grown. The radius of the cavity is bigger than the inscribed sphere but less than the circumscribed sphere of the PD to create an open cell lattice structure. Moreover, to reflect the experimental obtained struct geometry in Fig. 1(b), the radius of the cavity is chosen to be 1438.09 μm. In this way, the width of the cross-section area on the remaining open cell unit is ~ 174.89 μm; 3) upon the as-built PD structure with solid struts, a Ni wall with thickness from 10μm to 50μm are coated on the strut surface. Subsequently, the original solid core is removed to obtain the finalized HPD lattice in different wall thickness. Fig. 1(c&d) presents the HPD unit lattice geometry and the 3D packing 3×3×3 HPD lattice architecture.

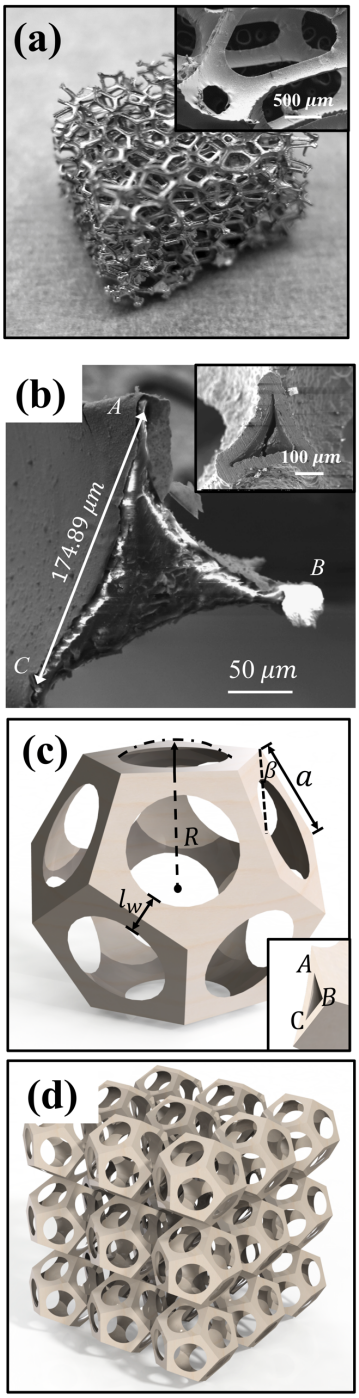

FIGURE 1: a) Optical image of the open-cell Ni foam, insert is the architecture of the copper coated PU foam as the template; b) Representative SEM image of a single strut in copper coated PU foam template, insert is the hollow Ni strut after template removal. c) A unit cell of HPD model and its lattice parameters. d) 3D packing of the HPD unit cells

Finite element method (FEM) simulations are performed in the commercial finite element code ANSYS to identify the stress concentration and distribution on the created HPD struts, which allows us not only to predict the location where the fracture, but also to estimate the elastic stiffness and derive the effective modulus as a function of relative density. All simulations were performed statically with linear perturbations to obtain the linear stiffness. The isotropic linear elastic materials model presented in Fig. 1(c), of which the general foam of Hooke's law is shown in equation (3), was used for the HPD simulations. The young's modulus of the homogeneous constituent Ni is set as 208 GPa [23]. Hollow strut unit cell simulations had around 120,000 elements. The exact number of elements varied depending on the type of the structure parameters (thickness, slenderness) used in the simulation. As largescale foam obtained in experiments requires prohibitively expensive computational times, to resolve this issue while keeping the accuracy of the computation, single HPD unit cell subject to periodic boundary conditions (PBCs) were utilized and manually imposed to obtain the effective stress and strain curve and also the effective stiffness of the full-scale geometry.

$$\begin{bmatrix}\epsilon_{11}\\ \epsilon_{22}\\ \epsilon_{33}\\ \epsilon_{12}\\ \epsilon_{13}\\ \epsilon_{23}\end{bmatrix} = \begin{bmatrix} 1/\mathrm{E} & -v/E & -v/E & 0 & 0 & 0\\ -v/E & 1/\mathrm{E} & -v/E & 0 & 0 & 0\\ -v/E & -v/E & 1/\mathrm{E} & 0 & 0 & 0\\ 0 & 0 & 0 & 1/\mathrm{G} & 0 & 0\\ 0 & 0 & 0 & 0 & 1/\mathrm{G} & 0\\ 0 & 0 & 0 & 0 & 0 & 1/\mathrm{G}\end{bmatrix}\begin{bmatrix}\sigma_{11}\\ \sigma_{22}\\ \sigma_{33}\\ \sigma_{12}\\ \sigma_{13}\\ \sigma_{23}\end{bmatrix} \quad (3)$$

For the uniaxial compression test, the bottom edge that is on the surface in contact with the stationary cylinder, was fixed in all principal directions. While the volume-averaged strain was imposed on the top edge. For the transverse components, PBC was manually enforced, by solving the relative displacements on the x- and y- edges, which is also used to avoid the effect of sliding during compression. The PBCs are imposed based on the following steps:

For the x axial:
Constrain on the for transverse displacement: $u_+^1 - u_-^1 = u^\delta$

Fix the in-plane displacement: $U_+^i = U_-^i, i = 2,3$

Repeat the process for the y and z edges.

, where $+$ and $-$ represent the two edges at the end along that direction. For the RVE unit cell, volume averaged strain δz is added along the z direction.

The compression simulations are carried out by linearly displacing the top surface along negative z direction through 50 sub steps until a total volume averaged strain of around 0.05 was reached. The simulations are only constrained to small deformation scale to avoid the plastic deformation and therefore to avoid bringing large computational error and the plastic deformation which is not the focus of this study. The effective modulus was calculated as the ratio between the averaged strain and the average stress of the unit cell along z-direction. Taking F to be the reaction force across the bottom edge, L to be the unit cell side length and δz to be the volume averaged strain, the modulus was calculated as equation (4).

$$E = \frac{\sigma_{ave}}{\epsilon_{ave}} = \frac{F}{L\delta z} \quad (4)$$

Fig. 2(b) presents a stress-strain curve result for $25\mu m$ wall thickness HPD lattice unit.

Beside of the mechanical modeling, in terms of calculating the effective thermal conductivity (ETC), a steady-state thermal resistance model is performed. The boundary conditions are arranged as follows: 1) temperature difference between two parallel ends of the HPD lattice unit was set to 1K as shown in Fig. 2(c) the other struts were set to be adiabatic. The FEM simulation employed the Ni properties at room temperature (300K). The convergence threshold was set to 10^{-13}, which was much lower than the default value 10^{-3} to ensure the accuracy. Only considering the conduction rate though Ni shell (Q_{cond}), FEM calculated k_{eff} as, $k_{eff} = \frac{Q_{cond}H}{A_{Ni,CS}(T_{top}-T_{bottom})}$, where T_{top} and T_{bottom} are the temperatures at the top and bottom edges. Since $T_{top} - T_{bottom}$ was equal to 1, and $A_{Ni,Cs}$ of HPD lattice is H^2. As a result, the above calculation can be reduced to $k_{eff} = Q_{cond}/H$. To make a comparison with experiment results, the HPD model with Ni thickness ranging from $10\mu m$ to $50\mu m$ are derived.

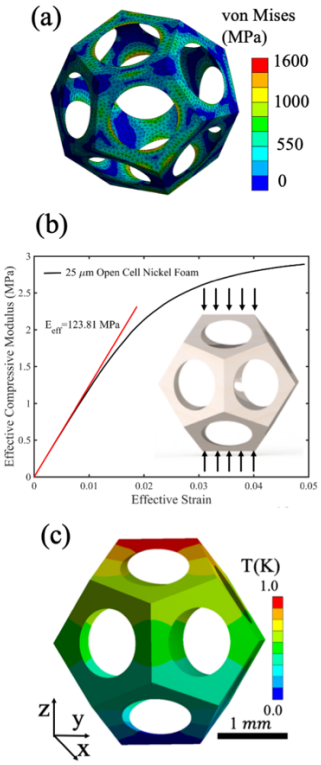

FIGURE 2: a) The stress contour of the HPD unit cell deformed under a series of volume averaged strains; b & c) engineering stress-strain curve and temperature contour plot of the HPD unit cell with wall thickness of $25\mu m$;

3. RESULTS AND DISCUSSION

3.1 Mechanical Property

Uniaxial compression experiments using Instron E3000 were conducted for our manuscript hollow struct Ni foam shown in Fig.1 (a). The elastic modulus is extracted by applying a linear least-squares fit to different small regions within the initial 2% strain and finding the maximum slope for each sample.

Cellular foam architectures either open-cell or closed-cell are often characterized by their relative density $\rho' = \rho/\rho_s$, where ρ is the foam and ρ_s is the density of the base materials [24]. Specifically, certain cellular material properties i.e., elastic stiffness, effective thermal conductivity, and the effective yield strength can be directly related to the properties of the material comprising the cell walls through the relative density [24].

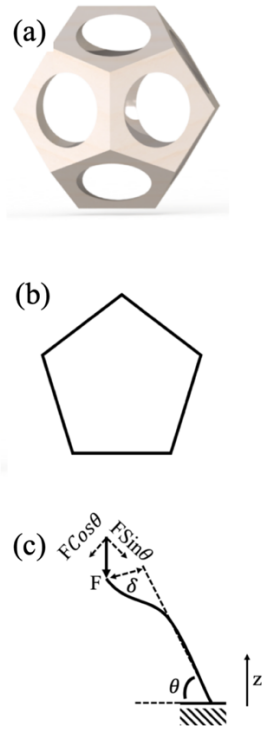

FIGURE 3: a) CAD model of the HPD lattice architecture. b) Equivalent non-rigid 2D unit cell of the 3D HPD lattice in A with the Cartesian coordinate system and loading force specified. c) Free body diagram of one-strut model under uniaxial free compression simplified using the symmetry property of the PD structure in B, while assuming the rigid boundary condition.

The material is assumed to be linear elastic and the stiffness of the HPD lattice architecture is studied using both the Euler-Bernoulli and Timoshenko beam theories [25, 26] to develop the analytical model specifically for the compressive response of the HPD lattice structure. For the 2D architecture, a lattice constructed with pure triangular are the strict rigid polygon. While for the 3D analogs, polyhedral lattices with fully triangulated surfaces are the strict rigid architecture. Therefore,

the node connectivity (Z) of a structure, which is the total average number of the struts connected at the node, are induced to explain the bending or stretching dominated structure. For our specific HPD lattice architecture shown in Fig. 3(a), as illustrated above, Z is 6 reflecting the bending dominated essential. To simplify the case, the generalized one strut model, shown in Fig. 3(b), is used to explain the non-rigid behavior of the HPD lattice. The following analysis based on the ideal HPD architecture with regular triangular cross-section, edge length c, length l, thickness h, and the constituent young's modulus E_s. As discussed previously, all the struts are subject to complex stress states and the combination of bending and stretching should be accounted for. Nodes and edges are all treated to be welded joints. What's more, the defects e.g. notch, misalignment, nodal compliance, and necking [27, 28] are neglected.

The effective stiffness of any architecture materials is defined as $S = F/\delta$, where δ is the effect deformation subject to the total force applied on the unit cell. As shown in Figure 3(c) and Figure 3D, the moment inertia is taken as I and oriented angle is θ.

According to the Euler-Bernoulli beam theory[25], the deflection of a clamped strut under load F_1 is:

$$\omega = \frac{F_1 l^3}{3EI} \tag{5}$$

Therefore, for the clamped strut AB, the deflection at point A can be calculated as:

$$\delta_{total} = \frac{Fl^3 \cos\theta}{12E_s I} \tag{6}$$

Then the deflection along the z direction is

$$\delta_{1z} = \frac{Fl^3 \cos^2\theta}{12E_s I} \tag{7}$$

For our hollow strut, its slenderness is pretty large resulting in a considerable shear deformation and based on the Timoshenko beam theory [26], the final deflection at the end is given as:

$$\omega = \frac{Fl^3}{3EI} + \frac{Fl}{\kappa AG} \tag{8}$$

, where κ is the Timoshenko shear coefficient within the range of [0.5,1], $G = \frac{E}{2(1+\nu)}$ represents the shear modulus, ν is the poisson's ratio and A is the cross-section area of the strut. Then the deflection at the end along z direction is:

$$\delta_{2z} = \frac{Fl\,(1+2\nu)\cos^2\theta}{\kappa AE} \tag{9}$$

Besides, the deformation along the axial of a beam caused by the axial force is give as:

$$\delta_3 = \frac{Flsin\theta}{E_s A} \tag{10}$$

Then the total deformation of the strut along z direction is

$$\begin{aligned}\delta &= \delta_{1z} + \delta_{2z} + \delta_{3z} \\ &= \frac{Fl^3\cos^2\theta}{12E_s I} + \frac{Fl\,(1+2\nu)\cos^2\theta}{\kappa AE_s} + \frac{Flsin^2\theta}{E_s A}\end{aligned} \tag{11}$$

And the stiffness for the non-rigid lattice architecture is calculated as:

$$S = \frac{E_s}{\frac{l^3}{12I}\cos^2\theta + \frac{l}{A}[\sin^2\theta + \frac{1}{\kappa}(1+2\nu)\cos^2\theta]} \tag{12}$$

For a generalized model, we have

$$S = \frac{E_s}{\frac{l^3}{I}\lambda_1 + \frac{l}{A}\lambda_2} \tag{13}$$

where C_1 and C_2 are the constants depending on the number of diagonal number of beams in the structure, and the inclined angle θ. Recall the effective modulus of the lattice architecture is calculated as $E = \frac{\sigma}{\epsilon} = S\frac{L_{edge}}{A_{eff}}$. The edge length of the unit cell and the effective surface area can be approximated with the length of the beam l as $L_{edge} \approx l\ and\ A_{eff} \approx l^2$ reducing the effective young's modulus as $E \approx S/l$.

Taken a regular triangular cross section, we have $I = \frac{\sqrt{3}}{96}(a^4 - (a-3h)^4) \approx \frac{\sqrt{3}}{96}(12a^3h)$ and $A \approx 3ah$. According to this, the effective young's modulus can be expressed as

$$E = \frac{E_s}{\frac{l^4}{a^3h}\lambda_1 + \frac{l^2}{ah}\lambda_2} \tag{14}$$

The relative density of the HPD unit cell with 30 struts can be approximated as $\rho' = \frac{V_{solid}}{V_{unit}} = \frac{90ahl}{18l^3} = \frac{5ah}{l^2}$, rewrite the effective young's modulus with respect to the relative density, we get

$$E = \frac{E_s}{\frac{1}{\rho'^2}\frac{h}{a}\lambda_1 + \frac{1}{\rho'}\lambda_2} \tag{15}$$

Also, noteworthy, $a \approx C.+3h \propto h$, and C. is the constant of the original edge length of the template (experiment) or the core (CAD model). According to this, the effective young's modulus can be reduced as

$$E = \frac{E_s}{\frac{1}{\rho'^2}\lambda_1 + \frac{1}{\rho'}\lambda_2} \tag{16}$$

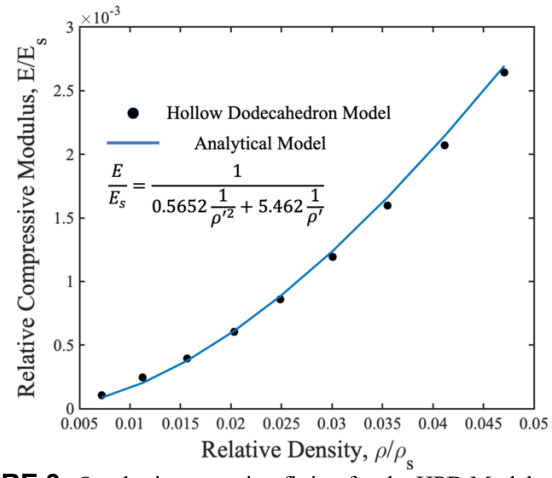

FIGURE 3: Quadratic regression fitting for the HPD Model

As an extreme case for very thin wall case ($\rho' \ll 1$), equation (16) approaches $\frac{E}{E_s} \approx \rho'^2 \frac{1}{\lambda 1}$, which is the idealized bending dominated relationship as the previous derived model by Gibson and Ashby[29]. For normal case, ρ' is always smaller than one resulting ρ'^2 dominated in the modulus equation, which implies the bending dominated behavior and partially explains the deviations of the power coefficient law. Moreover, as the layer become thicker, the strut in the HPD lattice structure cannot be simplified as beams due to the stress concentration at the edge of the inner circle on each pentagon surface and the contribution of beam intersecting at the node cannot be ignored as well, which are both key factors affecting the stiffness of HPD structure. As a result, the analytical model tends to break down. Based on these mathematical analyses, the proposed analytical model is valid for low relative densities, while nodal volume and bending corrections are needed to be considered for the large relative density structure. Our Analytical model are compared with the simulation result shown in Fig.3 showing great agreement.

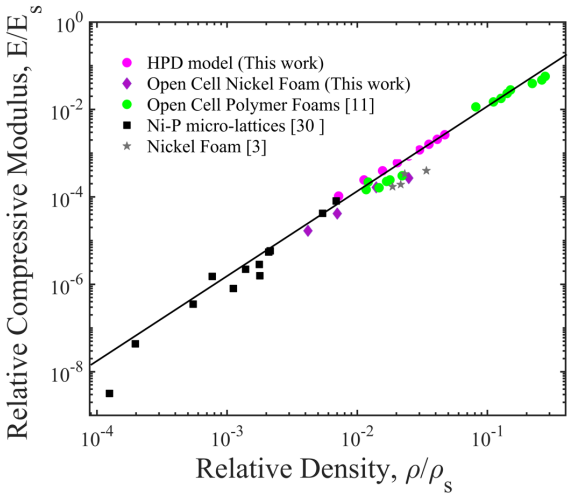

FIGURE 4: Relative compressive modulus (defined as the measured Young's modulus, E, divided by the Young's modulus of the constituent solid, E_s) of selected cellular materials at low relative density comparing to HPD model results.

The modulus of the as-manufactured open cell Ni foam is extracted and compared with the simulation results in Fig. 5. For comparison, the ultralight Ni micro-lattice [30], stochastic polymer foam [11] and Nickel foam prepared with pressure sintering [3] with relative density < 10 mg/cm^3 are plotted. As shown in Fig. 4, the obtained compressive modulus from the HPD models with relative density ranging from 0.01 to 0.1, performs a nonlinear mechanical property scaling in the factor of two, which is in great agreement with the experimental results. A small transition tendency captured in low density region (ρ_s~0.01) to a different, topology-dependent scaling relation is observed, which may be attributed to the defects in the real metallic foam architecture, i.e., waviness in the struts and non-uniform coating.

3.2 Thermal Property

Noteworthy, the actually effective thermal conductivity of the metal foam depends not only on the relative density and the thermal conductivity of the base materials constructing the foam architecture, but it also consistently related to the actual geometry of the foam as the conductivity pathways through the porous materials which are limited to the struts of the material.

If the thermal conductivity of the fluid phase is much smaller than that of foam structure. The effect of dispersion is negligible; while if it is comparable, the effect can be very pronounced and account for the final effective thermal transport.

The thermal conductivities of the foams were measured with TPS method at room temperature. Fig. 5(a) shows the measurement instrument (anisotropic module, TPS 2500S, Thermtest, Inc). A sensor (C5501, Thermtest, Inc) included a spiral-shape, 10μm-nickel foil, which was sandwiched by electrically insulating layers, 30μm thick polyimide (Kapton) film. The spiral area with a diameter of 12.8 mm generated Joule heating (Q), as the instrument supplied current over a predefined period of time (Δt). Sample width or diameter should be at least twice greater than the spiral diameter to ensure that the heat generated by the spiral area does not diffuse to the sample outside boundary within Δt. For the sampe reason, the sample thickness much be equal or greater than the spiral radius (r)

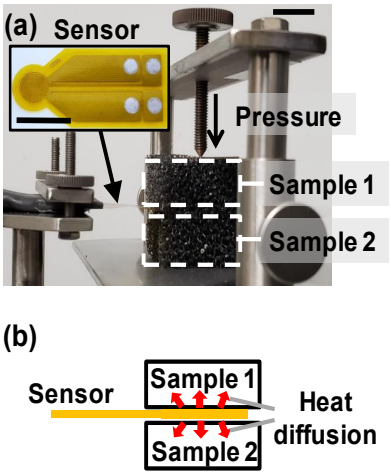

FIGURE 5: TPS instrument for measuring the thermal conductivity of the samples: a) photographic image (20mm bar for scale), and b) a schematic

An analytical approach, thermal resistance model, was developed to investigate the influence of the strut angular distribution and thermal transport path length on the open-cell composite foam ETC. The analytical model enables to study the effect of a specific model parameter with reduced computation cost as compared to FEM. Many semi-analytical models were introduced in literatures [31-35] to estimate the foam ETC while modeling the foam architecture as a periodic lattice structure. We adopted the edge by edge 3D packing architecture which was compatible with the HPD foam model [7].

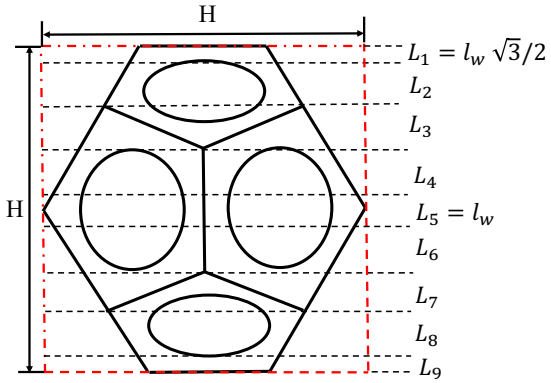

FIGURE 6: A representative unit volume, which is divided into 9 different layers considering the strut orientation.

In this approach, we divide the HPD lattice unit cell into 9 different layers and model them as a series of thermal resistances. Figure 6 illustrates how the unit cell is divided along the z axis which corresponds to the heat transfer direction in the model. This layer division is based on the strut angular distribution such that the angle between the strut and z axis [β as indicated in Fig. 1(c)] may possess only one or two values in each layer. Accordingly, the height of each layer (l_i) can be expressed with l, l_w, and dihedral angle of 58.3° by using the relations below, where the subscript i indicates the order of layer.

$$L_1 = L_9 = (\sqrt{3}l_w/2)\cos 58.3^o \quad (17)$$

$$L_2 = L_8 = (l - l_w)\cos 18^o \cos 58.3^o \quad (18)$$

$$L_3 = L_7 = l\cos 72^o \cos 58.3^o \quad (19)$$

$$L_4 = L_6 = (l - l_w)/2 \quad (20)$$

$$L_5 = l_w \quad (21)$$

The ETC of the open cell foam is often estimated using the volume averaged method [36], which can also be used to model the ETC of unit cell layers. Then the ETC of each layer ($k_{i,eff}$) is modeled as below [33].

$$k_{i,eff} = \varphi k_s \cos^2\beta + (1 - \varphi)k_f \quad (22)$$

, where k_s is the thermal conductivity and φ is the volume fraction of the solid skeleton. In Eq. (22), the second term on the right-hand side is assumed negligible, because $k_s >> k_f$. Then, based on the strut angular orientations of each layer, cosβ is determined as follows. For layers 1 and 8, cosβ = 1. For layers 2 and 7, cosβ = cos18°cos58.3°. For layers 3 and 6, cosβ = cos72°cos58.3°. For layers 4 and 5, cosβ is 1 for the orthogonal struts and cos18°cos58.3° for the tilted strut. The volume fraction φ is calculated by the strut volume divided by the layer envelope volume (V_i), where $V_i = L_i H^2$.

Considering that the struts can be shared by more than one unit cell in lattice, the number and volume of struts are determined as follows. Layers 1 and 9 include 1 complete horizontal strut each. Layers 2 and 8 include 4(l–l_w)cos18°cos58.3° struts each. In layers 3 and 7, there are 4 + 4(1 - ε) struts in total, where ε = 0.5l/(0.5H - lcos18°cos58.3°). In layers 4 and 6, there are (l -l_w) + 4(ε - l_w/l) struts in total. Layer 5 includes 2 + 2lw/l struts. Thus, each unit cell possesses 30 struts in total. If the volume of a single strut is expressed as Vt/30, where Vt is the total volume of struts per unit cell, then $k_{i,eff}$ is calculated layer by layer:

$$k_{1,eff} = k_{9,eff} = \frac{1}{30}\frac{V_t}{V_1}k_s \quad (23)$$

$$k_{2,eff} = k_{8,eff} = \frac{2}{15}\frac{V_t}{V_2}k_s(\cos 18^o \cos 58.3^o)^2\, k_s \quad (24)$$

$$k_{3,eff} = k_{7,eff} = \frac{2}{15}\frac{V_t}{V_3}(\cos 72^o \cos 58.3^o)^2 k_s + \frac{2}{15}(1-\epsilon)\frac{V_t}{V_3}(cos18^o cos58.3^o)^2 k_s \quad (25)$$

$$k_{4,eff} = k_{6,eff} = \frac{1}{30}\frac{V_t}{V_4}\frac{l-l_w}{l}k_s + \frac{2}{15}(\epsilon\frac{V_t}{V_4} - \frac{l_w}{l}\frac{V_t}{V_4})(\cos 18^o \cos 58.3^o)^2 k_s \quad (26)$$

$$k_{5,eff} = \frac{1}{15}\frac{l_w}{l}\frac{V_t}{V_5}k_s + \frac{1}{15}\frac{V_t}{V_5}k_s \quad (27)$$

For the thermal resistances in series, the total thermal resistance is the sum of constituents. Accordingly, the ETC of an HPD unit cell is obtained as below.

$$k_{eff} = H/[\frac{2(l_w\sqrt{3}/2)\cos 58.3^o}{k_{1,eff}} + \frac{2(l-l_w)\cos 18^o \cos 58.3^o}{k_{2,eff}} + \frac{2l\cos 72^o \cos 58.3^o}{k_{3,eff}} + \frac{(l-l_w)/2}{k_{4,eff}} + \frac{l_w}{k_{5,eff}}] \quad (28)$$

Fig. 7 shows the predicted k_{eff} by Eq. 28.

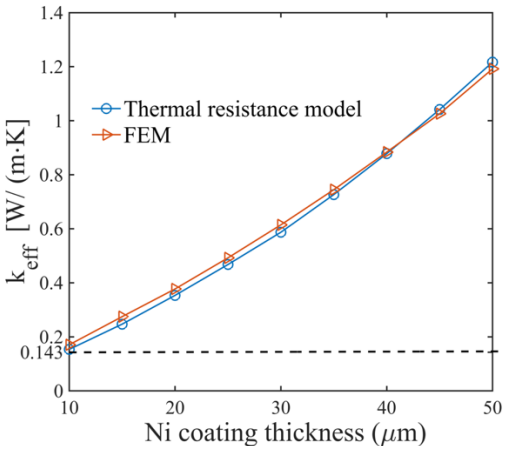

FIGURE 7: The ETC of the HPD architecture predicted by FEM and the thermal resistance model as a function of Ni coating thickness. The black dash line indicates the experiment result, corresponding to ETC=0.143 W/(mK) and the thickness is ~10μm.

Although our simplified model has proved to be effectively estimate the thermal properties of stochastic foam architecture, it is clear that detailed modeling of the flow and heat transfer behavior for a realistic foam architecture should lead to further improvement of both the heat transfer performance and the optimization of the geometry.

4. CONCLUSION

Cellular foams offer advantages over conventional structures for both mechanical and thermal applications. Especially when coating metal layer conformably onto polymer foam templates, these manufactured core-shell composite foams or foams with hollow struts (after polymer templates removal) have demonstrated successful applications in many fields, such as energy absorption, heat exchanger, and among others. To understand the physical properties of these foams, a newly developed 3D packing HPD lattice architecture is proposed in this study. With corresponding FEM thermal and mechanical simulations, it has been demonstrated to have a good agreement with experiment result for predicting both the mechanical properties and thermal properties of the hollow metallic foam architecture. For the mechanical property, our HPD model not only provides an insight explanation of the parameter space of hollow struts-cellular architecture but also establishes mechanism of the strength and the stiffness governed by the intricate entanglement. With respect to the thermal transport property, using the HPD model, it clearly identified the deterministic parameters of the foam architecture, i.e., strut angular distribution and thermal transport path length. It is believed that the HPD model are capable for aiding the novel foam design in various field.

Like other developed conventional models, there are still some limitations. Although our HPD model greatly simplified the modeling process, which exceeds other modeling especially for the stochastic hollow foam-based architectures, when applying the HPD lattice model, it is still necessary to verify that the assumptions on which they are based such as local thermal equilibrium, negligible thermal dispersion, slenderness beam, low density are valid. Also, for the node effect, more accurate model may be needed to be developed. To conclude, the present HPD models provides scientific insight to harness the comprehended knowledge on the geometry topology to understand the physical properties of the foam-based architecture.

ACKNOWLEDGEMENTS

This study is partially supported by ASU startup funds, Salt River Project (SRP) Research Grant Program, and NSF grant CMMI-1826439. We acknowledge the use of facilities within the Eyring Materials Center at Arizona State University supported in part by NNCI-ECCS-1542160. The Instron E3000 was obtained using funds from the Army Research Office (W911NF-15-1-0353).

REFERENCES

[1] Paulose, J., Meeussen, A. S., and Vitelli, V., 2015, "Selective buckling via states of self-stress in topological metamaterials," Proc. Natl. Acad. Sci., 112(25), pp. 7639-7644.

[2] Davies, G. J., and Zhen, S., 1983, "Metallic foams: their production, properties and applications," J. Mater. Sci., 18(7), pp. 1899-1911.

[3] Shbeh, M. M., and Goodall, R., 2016, "Open pore titanium foams via metal injection molding of metal powder with a space holder," Met. Powder Rep., 71(6), pp. 450-455.

[4] Queheillalt, D. T., Hass, D. D., Sypeck, D. J., and Wadley, H. N. G., 2001, "Synthesis of open-cell metal foams by templated directed vapor deposition," J. Mater. Res., 16(4), pp. 1028-1036.

[5] Rashed, M. G., Ashraf, M., Mines, R. A. W., and Hazell, P. J., 2016, "Metallic microlattice materials: A current state of the art on manufacturing, mechanical properties and applications," Mater. Des, 95, pp. 518-533.

[6] Gu, G. X., and Buehler, M. J., 2018, "Tunable mechanical properties through texture control of polycrystalline additively manufactured materials using adjoint-based gradient optimization," Acta Mechanica, 229(10), pp. 4033-4044 %@ 0001-5970.

[7] Dai, R., Wang, M., Wang, D., Hu, Z., Green, M. D., and Nian, Q., 2020, "Understanding mechanical behavior of metallic foam with hollow struts using the hollow pentagonal dodecahedron model," Scr. Mater., 182, pp. 114-119

[8] Han, X.-H., Wang, Q., Park, Y.-G., T'Joen, C., Sommers, A., and Jacobi, A., 2012, "A Review of Metal Foam and Metal Matrix Composites for Heat Exchangers and Heat Sinks," Heat Transfer Eng., 33(12), pp. 991-1009.

[9] Han, S. C., Lee, J. W., and Kang, K., 2015, "A new type of low density material: Shellular," Adv. Mater., 27(37), pp. 5506-5511 %@ 0935-9648.

[10] Freyman, T. M., Yannas, I. V., and Gibson, L. J., 2001, "Cellular materials as porous scaffolds for tissue engineering," Progress in Materials science, 46(3-4), pp. 273-282 %@ 0079-6425.

[11] Gibson, I. J., and Ashby, M. F., 1982, "The mechanics of three-dimensional cellular materials," Proc. R. Soc. Lond. A, 382(1782), pp. 43-59.

[12] Schaedler, T. A., Jacobsen, A. J., Torrents, A., Sorensen, A. E., Lian, J., Greer, J. R., Valdevit, L., and Carter, W. B., 2011, "Ultralight metallic microlattices," Science, 334(6058), pp. 962-965.

[13] Li, R., Wang, S., Huang, Z., Lu, F., and He, T., 2016, "NiCo2S4@ Co (OH) 2 core-shell nanotube arrays in situ grown on Ni foam for high performances asymmetric supercapacitors," J. Power Sources, 312, pp. 156-164

[14] Shi, H., Shi, D., Yin, L., Yang, Z., Luan, S., Gao, J., Zha, J., Yin, J., and Li, R. K. Y., 2014, "Ultrasonication assisted preparation of carbonaceous nanoparticles modified polyurethane foam with good conductivity and high oil absorption properties," Nanoscale, 6(22), pp. 13748-13753.

[15] Yang, W., Luo, S., Zhang, B., Huang, Z., and Tang, X., 2008, "Electroless preparation and characterization of magnetic Ni–P plating on polyurethane foam," Appl. Surf. Sci., 254(22), pp. 7427-7430.

[16] Warren, W. E., and Kraynik, A. M., 1997, "Linear elastic behavior of a low-density Kelvin foam with open cells," J. Appl. Mech., 64(4), pp. 787-794.

[17] Buffel, B., Desplentere, F., Bracke, K., and Verpoest, I., 2014, "Modelling open cell-foams based on the Weaire--Phelan unit cell with a minimal surface energy approach," Int. J. Solids Struct., 51(19-20), pp. 3461-3470.

[18] Kwon, Y. W., Cooke, R. E., and Park, C., 2003, "Representative unit-cell models for open-cell metal foams with or without elastic filler," Mater. Sci. Eng. A, 343(1-2), pp. 63-70.

[19] Petit, C., Maire, E., Meille, S., and Adrien, J., 2017, "Two-scale study of the fracture of an aluminum foam by X-ray tomography and finite element modeling," Mater. Des, 120, pp. 117-127.

[20] Boomsma, K., Poulikakos, D., and Ventikos, Y., 2003, "Simulations of flow through open cell metal foams using an idealized periodic cell structure," Int. J. Heat Fluid Flow, 24(6), pp. 825-834.

[21] Wang, M., and Pan, N., 2008, "Modeling and prediction of the effective thermal conductivity of random open-cell porous foams," Int. J. Heat Mass Transfer, 51(5-6), pp. 1325-1331

[22] Xiao, X., Zhang, P., and Li, M., 2014, "Effective thermal conductivity of open-cell metal foams impregnated with pure paraffin for latent heat storage," International Journal of Thermal Sciences, 81, pp. 94-105

[23] Jung, A., and Diebels, S., 2016, "Synthesis and mechanical properties of novel Ni/PU hybrid foams: a new economic composite material for energy absorbers," Adv. Eng. Mater., 18(4), pp. 532-541.

[24] Ashby, M. F., Evans, T., Fleck, N. A., Hutchinson, J. W., Wadley, H. N. G., and Gibson, L. J., 2000, Metal foams: a design guide, Elsevier.

[25] Young, W. C., Budynas, R. G., and Sadegh, A. M., 2002, Roark's formulas for stress and strain, McGraw-Hill New York.

[26] Timoshenko, S., 1970, "P, and Goodier, JN Theory of Elasticity," McGraw Hill.

[27] Amsterdam, E., Onck, P. R., and De Hosson, J. T. M., 2005, "Fracture and microstructure of open cell aluminum foam," J. Mater. Sci., 40(22), pp. 5813-5819 %@ 0022-2461.

[28] Amsterdam, E., De Vries, J. H. B., De Hosson, J. T. M., and Onck, P. R., 2008, "The influence of strain-induced damage on the mechanical response of open-cell aluminum foam," Acta Mater., 56(3), pp. 609-618 %@ 1359-6454.

[29] Gibson, I. J., and Ashby, M. F., 1982, "The mechanics of three-dimensional cellular materials," Proc. R. Soc. Lond. A, 382(1782), pp. 43-59

[30] Torrents, A., Schaedler, T. A., Jacobsen, A. J., Carter, W. B., and Valdevit, L., 2012, "Characterization of nickel-based microlattice materials with structural hierarchy from the nanometer to the millimeter scale," Acta Mater., 60(8), pp. 3511-3523

[31] Calmidi, V. V., and Mahajan, R. L., 1999, "The effective thermal conductivity of high porosity fibrous metal foams," J. Heat Transfer, 121(2).
[32] Boomsma, K., and Poulikakos, D., 2001, "On the effective thermal conductivity of a three-dimensionally structured fluid-saturated metal foam," Int. J. Heat Mass Transfer, 44(4), pp. 827-836.
[33] Dai, Z., Nawaz, K., Park, Y. G., Bock, J., and Jacobi, A. M., 2010, "Correcting and extending the Boomsma–Poulikakos effective thermal conductivity model for three-dimensional, fluid-saturated metal foams," Int. Commun. Heat Mass, 37(6), pp. 575-580
[34] Yang, X. H., Bai, J. X., Yan, H. B., Kuang, J. J., Lu, T. J., and Kim, T., 2014, "An analytical unit cell model for the effective thermal conductivity of high porosity open-cell metal foams," Transport Porous Media, 102(3), pp. 403-426
[35] Baillis, D., Coquard, R., and Cunsolo, S., 2017, "Effective conductivity of Voronoi's closed-and open-cell foams: Analytical laws and numerical results," J. Mater. Sci., 52(19), pp. 11146-11167
[36] Kaviany, M., 2012, Principles of heat transfer in porous media, Springer Science & Business Media.